

Challenging claims of “elliptic flow” by comparing azimuth quadrupole and jet-related angular correlations from Au-Au collisions at $\sqrt{s_{NN}} = 62$ and 200 GeV

Thomas A. Trainor, David T. Kettler, and Duncan J. Prindle
 CENPA 354290, University of Washington, Seattle, WA 98195

R. L. Ray

Department of Physics, University of Texas at Austin, Austin, TX 78712

(Dated: March 14, 2019)

Background: A component of azimuth correlations from high-energy heavy ion collisions varying as $\cos(2\phi)$ and denoted by symbol v_2 is conventionally interpreted to represent “elliptic flow,” a hydrodynamic manifestation of the initial-state A-A overlap geometry. Several numerical methods are used to estimate v_2 , resulting in various combinations of “flow” and “nonflow” that reveal systematic biases in the v_2 estimates. QCD jets contribute strongly to azimuth correlations and specifically to the $\cos(2\phi)$ component. **Purpose:** We question the extent of jet-related (“nonflow”) bias in and hydrodynamic “flow” interpretations of v_2 measurements. **Method:** We introduce two-dimensional (2D) model fits to angular correlation data that distinguish accurately between jet-related correlation components and a *nonjet azimuth quadrupole* that might represent “elliptic flow” if that were relevant. We compare measured jet-related and “flow”-related data systematics and determine the jet-related contribution to v_2 measurements. **Results:** Jet structure does introduce substantial bias to conventional v_2 measurements, making interpretation difficult. The nonjet quadrupole exhibits very simple systematics on centrality and collision energy—the two variables factorize. Within a Au-Au centrality interval where jets show no indication of rescattering or medium effects the nonjet quadrupole amplitude rises to 60% of its maximum value. **Conclusions:** Disagreements between nonjet quadrupole systematics and hydro theory expectations, the large quadrupole amplitudes observed in more-peripheral Au-Au collisions and a significant nonzero value in N-N $\approx p$ -p collisions strongly suggest that the nonjet quadrupole does not arise from a hydrodynamic “flow” mechanism.

PACS numbers: 13.66.Bc, 13.87.-a, 13.87.Fh, 12.38.Qk, 25.40.Ep, 25.75.-q, 25.75.Gz

I. INTRODUCTION

Measurements of a Fourier component of the “azimuthal anisotropy” of particle momenta in RHIC heavy ion collisions have been interpreted to indicate production of a thermalized QCD medium with low viscosity, frequently invoked as evidence for a “perfect liquid” (e.g., [1, 2]). That conclusion is based on a conventional interpretation of the $v_2 = \langle \cos(2\phi) \rangle$ anisotropy component as a measure of elliptic flow, a conjectured hydrodynamic (hydro) response to density and pressure gradients in the initial collision system corresponding to the transverse eccentricity of the A-A overlap region [3]. In a hydro context large elliptic flow values combined with other measurements are interpreted to imply large energy densities, rapid thermalization and small viscosities [4, 5].

However, questions persist concerning v_2 measurements, their accuracy and their interpretation. Conventional v_2 measurements [6] do not distinguish accurately between an isolated *azimuth quadrupole* ($m = 2$ cylindrical multipole) Fourier component conjectured to represent elliptic flow and “nonflow”—a catch-all term representing several possible contributions to v_2 , but mainly the $m = 2$ azimuth Fourier component of a two-dimensional (2D) peak attributed to jets [7–11]. Whatever the precision of v_2 measurements the physical phenomena actually represented by any $\cos(2\phi)$ asymmetry measurement can be questioned [12, 13].

Conventional quadrupole measures $v_2\{\text{method}\}$ motivated from a hydro context [3] are difficult to interpret, and the statistical properties of some v_2 methods lead to substantial systematic bias. In Ref. [14] it was shown that event-plane $v_2\{\text{EP}\}$ [6] is a close approximation to two-particle cumulant $v_2\{2\}$ [15], in turn equivalent to the $m = 2$ Fourier coefficient of a projection of all angular correlations onto 1D azimuth [see Eq. (1)], which may include a large contribution from a prominent 2D peak interpreted in a perturbative QCD (pQCD) context as representing minimum-bias jet structure [7, 16–19]. Four-particle cumulant $v_2\{4\}$ [20, 21] reduces, but does not necessarily eliminate, the jet-related contribution [55]. Other model-dependent strategies have been invoked in attempts to reduce the “nonflow” (jet) contribution to v_2 , but the effectiveness remains uncertain [13, 22].

An alternative method introduced in Ref. [23] employs physical-model-independent analysis to isolate *geometrically* the *nonjet* azimuth quadrupole from other contributions. Nonjet (NJ) quadrupole amplitudes are obtained from fits to 2D angular correlations on azimuth ϕ and pseudorapidity η . Measurements of the NJ quadrupole over all Au-Au centralities and a large energy interval provide qualitatively new insights into the quadrupole phenomenon conventionally attributed to elliptic flow. NJ quadrupole amplitudes obtained with 2D model fits follow simple trends on centrality and energy described by just two initial-state parameters for all systems down to $\sqrt{s_{NN}} = 13$ GeV.

The quadrupole analysis method introduced in Ref. [23] is based on algebraic study of v_2 methods in Refs. [13, 14] and initial experience with 130 GeV data in Refs. [8, 24] where general model-fit analysis of 2D angular autocorrelations was first introduced. The same model-fit method was refined and elaborated in Ref. [7] where the primary focus was the energy and centrality systematics of angular correlations attributed to minimum-bias jets or *minijets*. The present study combines the numerical results of Refs. [7, 23] to examine the systematic relation between the NJ quadrupole and minijets and to test the validity of the conventional “elliptic flow” interpretation for the former.

In this study we examine the distinction between non-jet and jet-related quadrupole contributions in relation to other correlation structure. We review the centrality and energy dependence of the NJ quadrupole in terms of Glauber-model parameters as reported in Ref. [23] and contrast those trends with minijet systematics as established in Ref. [7]. We compare NJ quadrupole results with previous v_2 measurements and with hydro expectations. We conclude that NJ quadrupole variations on energy above 13 GeV and all Au-Au centralities are remarkably simple. Those trends and comparisons with minijet systematics appear to contradict conventional hydro expectations for elliptic flow. For example, the NJ quadrupole increases to 60% of its maximum value within a Au-Au centrality interval where the lowest-energy-jet-related correlations are consistent with a transparent collision system, as explained below.

This article is organized as follows: Sec. II reviews analysis methods applied to 2D angular correlations and “flow” analysis. Sec. III presents measured angular correlations and 2D model fits. Sec. IV reviews model-fit results for jet-related and nonjet quadrupole correlation components and a universal parametrization of energy and centrality dependence for the latter. Sec. V compares nonjet quadrupole and jet-related trends in the context of hydrodynamic expectations for the former. Sec. VI presents a discussion of selected results, and Sec. VII summarizes

II. ANALYSIS METHODS

A major emphasis of this study is accurate distinction between jet-related and nonjet quadrupole components of angular correlations and the energy and centrality systematics of the latter—what those imply for physical interpretation of the nonjet quadrupole phenomenon. We examine the underlying assumptions and systematic uncertainties of the model-fit analysis method in comparison with alternative v_2 analysis methods that seem to support flow interpretations.

A. Correlation spaces

Two-particle correlations are structures in the pair density on 6D momentum space $(p_{t1}, \eta_1, \phi_1, p_{t2}, \eta_2, \phi_2)$ that deviate from some defined reference density. In this analysis we study p_t -integral correlations on angular subspace $(\eta_1, \phi_1, \eta_2, \phi_2)$, where the angle parameters for relativistic collisions are pseudorapidity η (related to polar angle θ) and azimuth ϕ . We can reduce $(\eta_1, \phi_1, \eta_2, \phi_2)$ to a viewable 2D space with no significant loss of correlation information by using *angular autocorrelations* [25].

An autocorrelation as conventionally defined is derived from a pair density $\rho(x_1, x_2)$ by averaging along diagonals in space (x_1, x_2) parallel to sum axis $x_\Sigma = x_1 + x_2$. The averaged pair density $\rho(x_\Delta)$ on difference axis $x_\Delta = x_1 - x_2$ is then an autocorrelation [25]. For correlation structure approximately uniform on x_Σ (“stationarity”), typical over 2π azimuth and within a limited pseudorapidity acceptance $\Delta\eta$, angular correlations remain undistorted [24]. Within the STAR time projection chamber (TPC) acceptance [26] 2D angular autocorrelations are lossless projections of p_t -integral two-particle momentum space onto subspace $(\eta_\Delta, \phi_\Delta)$ [14]. The ϕ_Δ axis is divided into *same-side* (SS, $|\phi_\Delta| < \pi/2$) and *away-side* (AS, $\pi/2 < |\phi_\Delta| < \pi$) intervals.

B. Correlation measures

There are several alternatives for the definition of a correlation measure. The basic element is a histogram of covariances representing correlations of event-wise fluctuations between pairs of 2D bins on (η, ϕ) . $\Delta\rho = \rho - \rho_{ref}$ represents a covariance density, where object pair density ρ contains the structure of interest and reference density ρ_{ref} may be defined in terms of a factorization assumption or constructed from mixed-event pairs.

Per-pair density ratio $\Delta\rho/\rho_{ref} = \rho_{sib}/\rho_{mix} - 1$ (sometimes referred to as a “correlation function” and denoted by C) varies with system size as $1/n_{ch}$ (n_{ch} is charge multiplicity) absent other physical changes. ρ_{sib} and ρ_{mix} represent sibling (same-event) pairs and mixed-event pairs. In previous analysis we introduced a statistical measure whose variation with n_{ch} reflects only nontrivial physical changes in correlations, the *per-particle density ratio* $\Delta\rho/\sqrt{\rho_{ref}}$ (Pearson’s normalized covariance [27, 28] converted to a density ratio) that exhibits the desired properties, since $\sqrt{\rho_{ref}} \propto n_{ch}$ [7, 9, 10, 25]. We introduce previous correlation measurements in terms of that measure. We also reconsider what “particle” type best serves as a scaling reference in a given context—final-state hadrons as in $\Delta\rho/\sqrt{\rho_{ref}}$, initial-state participant nucleons or the number of N-N binary collisions—and rescale some of the correlation data accordingly.

C. Two-dimensional correlation model

Inspection of the 2D data histograms reveals that p_t -integral pair-density difference $\Delta\rho(\eta_\Delta, \phi_\Delta)$ contains two types of structure: η_Δ -dependent 1D and 2D peaks and η_Δ -independent sinusoids $\cos(\phi_\Delta)$ and $\cos(2\phi_\Delta)$, where the $\cos(2\phi_\Delta)$ sinusoid (quadrupole) can be related to v_2 measurements. We therefore define a model of 2D angular correlations that includes a part varying with η_Δ (2D) and a part independent of η_Δ (1D) composed of the $m = 1, 2$ terms of a (truncated) Fourier series

$$\frac{\Delta\rho}{\sqrt{\rho_{\text{ref}}}} \equiv \frac{\Delta\rho_{2\text{D}}}{\sqrt{\rho_{\text{ref}}}}(\eta_\Delta, \phi_\Delta) + 2 \sum_{m=1}^2 \frac{\Delta\rho[m]}{\sqrt{\rho_{\text{ref}}}} \cos(m\phi_\Delta). \quad (1)$$

No higher terms in the Fourier series are *required* by the data [7, 22, 29]. Fourier coefficients $\Delta\rho[m]/\sqrt{\rho_{\text{ref}}} = V_m^2/2\pi n$ include *power-spectrum* elements $V_m^2 = \sum_{i \neq j}^{n, n-1} \cos(m[\phi_i - \phi_j]) \equiv n(n-1)\langle \cos(m\phi_\Delta) \rangle$ [14], where n is the multiplicity in one unit of η and 2π azimuth, so $n/2\pi \approx d^2 n_{ch}/d\eta d\phi \equiv \rho_0$. Angle brackets denote event-wise means. The first term $\Delta\rho_{2\text{D}}/\sqrt{\rho_{\text{ref}}}$ is a combination of 1D and 2D peaked functions (Gaussians) [7]. $V_2^2/2\pi n \equiv \rho_0 v_2 \{2D\}^2 \equiv A_Q \{2D\}$ defines *quadrupole* measure $v_2 \{2D\}$ as a variant of conventional v_2 measures which would coincide approximately with $v_2 \{2\}$ in the absence of jets but which continues to measure a *nonjet* quadrupole (not associated with the SS 2D peak) to the statistical limits of data in the presence of jets [13]. The 2D correlation model is not motivated by physical interpretations of correlation structure elements. The detailed fit model is defined explicitly in Sec. III B.

D. “Flow” and “nonflow”

Conjectured elliptic flow, a possible hydrodynamic response to initial pressure/density gradients and overlap geometry in non-central A-A collisions, is assumed to be measured by the quadrupole ($m = 2$) term in a Fourier-series decomposition of the entire final-state azimuth distribution [6]. The $m = 2$ Fourier coefficient is commonly represented by symbol v_2 . Fourier analysis is applied to all azimuth structure (“anisotropy”) assuming that elliptic flow dominates that structure. However, possible “nonflow” (non-hydrodynamic) contributions to v_2 are admitted. A variety of schemes has been introduced to detect and reduce “nonflow” bias. However, considerable uncertainty remains for conventional v_2 methods [15]. Distinctions between “flow” and “nonflow” have been extensively discussed (e.g., Refs. [13, 15, 22]).

The assumptions that support such terminology can be questioned. Minimum-bias jets contribute strongly to “azimuthal anisotropy,” are predicted for high-energy nuclear collisions and must form a substantial contribution to “nonflow.” And the nonjet contribution to v_2 may not in fact be a flow phenomenon. In the present context we

refer instead to a nonjet quadrupole (what might be attributed to elliptic flow) and a jet-related quadrupole (v_2 contribution mainly from jets and mainly from a prominent SS 2D peak in 2D angular correlations).

It has been demonstrated that 2D model fits to angular correlations distinguish jet-related structure from the NJ quadrupole with few-percent accuracy [7, 13, 14, 23, 30]. As noted, the model functions used in the 2D model fits are motivated by empirical observations of data structure, not physical interpretations of structure components [7–9, 13, 14]. The accurate separation of NJ quadrupole and jet-related components by means of 2D model fits and estimates of jet-related bias (“nonflow”) in published v_2 measurements obtained with conventional “flow” methods are discussed further in App. A

E. Centrality measures

Several centrality measures can be related to observed charge multiplicity n_{ch} within some angular acceptance ($\Delta\eta, \Delta\phi$) based on the Glauber model of A-A collisions [31]. The common element is the fractional cross section $\sigma/\sigma_0 \equiv b^2/b_0^2$ inferred experimentally from the measured minimum-bias event distribution on n_{ch} .

Glauber Monte Carlo parameters N_{part} (number of participant projectile nucleons N) and N_{bin} (N-N binary collisions) (with 200 GeV N-N cross section $\sigma_{NN} = 42$ mb assumed) are related to n_{ch} within the STAR TPC acceptance. Centrality measure $\nu \equiv 2 N_{bin}/N_{part}$ in turn estimates the mean number of N-N binary collisions per participant pair (mean participant path length). We retain the same 200 GeV Glauber parameters for all energies as purely geometrical measures of A-A centrality.

F. Two-component model

The two-component model (TCM) of hadron production near mid-rapidity in high-energy nuclear collisions is based on a hypothesis of two dominant production mechanisms: (a) projectile nucleon dissociation (soft) and (b) large-angle-scattered parton fragmentation to jets (hard) [32]. The TCM is observed to provide a consistent quantitative description of p_t spectra and correlations [7, 16–19, 33]. In more-peripheral A-A collisions exhibiting *Glauber linear superposition* (GLS) of N-N collisions the soft component should scale $\propto N_{part}$, and the hard component (dijet production) should scale $\propto N_{bin}$.

As noted, pair-density difference $\Delta\rho$ represents a covariance histogram. If the covariance does not change with centrality the ratio $\Delta\rho/\sqrt{\rho_{\text{ref}}}$ then scales $\propto 1/n_{ch}$. However, $\Delta\rho$ may include contributions from several mechanisms with their own scaling behaviors. The soft component of $\Delta\rho/\sqrt{\rho_{\text{ref}}}$ should scale as N_{part}/n_{ch} and the hard component as $N_{bin}/n_{ch} = \nu \times N_{part}/2n_{ch}$. That is just the scaling observed within the GLS centrality region of Au-Au collisions for soft and hard components of

2D angular correlations measured by $\Delta\rho/\sqrt{\rho_{ref}}$ [7].

We can test the TCM more precisely by rescaling the fit-model amplitudes used to describe $\Delta\rho/\sqrt{\rho_{ref}}$ with the appropriate factors, either n_{ch}/N_{part} (soft) or n_{ch}/N_{bin} (hard). If the rescaled data are invariant on centrality over some interval we conclude that the GLS condition does persist there and that the assumed soft- or hard-component scaling designation is correct. Rescaling results are shown in Sec. V.

III. 2D ANGULAR AUTOCORRELATIONS

We describe data volumes, example 2D data histograms, principal features of the angular correlations and fitting procedures used to derive jet-related and non-jet quadrupole energy and centrality systematics.

A. Data histograms

The analyses reported in Refs. [7, 23] were based on 6.7M and 1.2M Au-Au collisions at $\sqrt{s_{NN}} = 62.4$ (year 2004) and 200 GeV (year 2001) respectively, observed with the STAR TPC. The momentum acceptance was defined by transverse momentum $p_t > 0.15$ GeV/c, pseudorapidity $|\eta| < 1$ and 2π azimuth. Au-Au collision centrality was defined as in Ref. [31]. Minimum-bias event samples were divided into 11 centrality bins: nine $\sim 10\%$ bins from 100% to 10%, the last 10% divided into two 5% bins. The corrected centrality of each bin as modified by tracking and event vertex inefficiencies was determined with a running-integral procedure. Centralities from N-N collisions to central Au-Au were thereby determined to about 2% uncertainty.

Figure 1 (left panels) shows 200 GeV 2D angular correlations for (corrected) 83-93% (\approx N-N collisions) and 0-5% centrality bins. Angular correlations for 62 GeV have similar features but with quantitative differences. Within the STAR TPC acceptance the minimum-bias correlation data from Au-Au collisions include three principal components: (a) a same-side (SS) 2D peak at the origin on $(\eta_\Delta, \phi_\Delta)$ well approximated by a 2D Gaussian for all minimum-bias data, (b) an away-side (AS) 1D peak on azimuth or “ridge” well approximated by AS azimuth dipole $[1 - \cos(\phi_\Delta)]/2$ for all minimum-bias data and uniform to a few percent on η_Δ (having negligible curvature), and (c) an azimuth quadrupole $\cos(2\phi_\Delta)$ also uniform on η_Δ to a few percent over the full angular acceptance of the STAR TPC. Other components consist of a sharp 2D exponential peak at (0,0) and a narrow 1D peak on η_Δ . That phenomenological description does not rely on any physical interpretation of the components.

Based on comparisons of observed data systematics with theory the components (a) and (b) together have been interpreted to represent minimum-bias jets or mini-jets [7, 17]. Component (c), identified as the nonjet azimuth quadrupole, has been conventionally attributed to

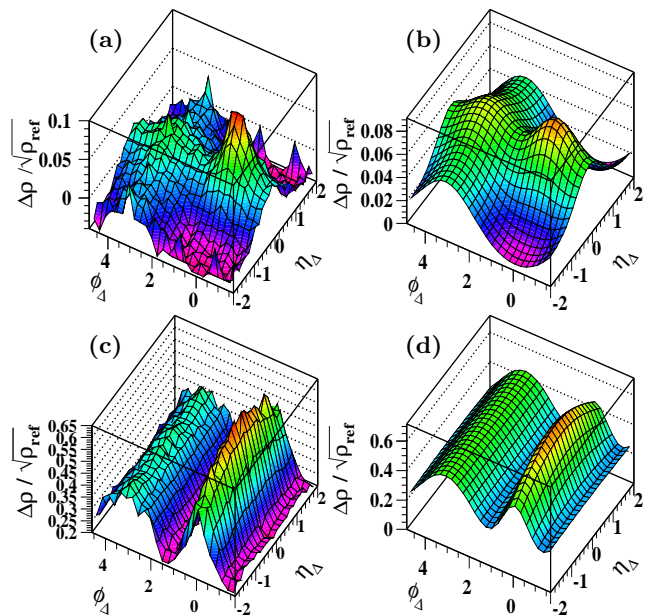


FIG. 1: (Color online) Left: 2D angular autocorrelations for 200 GeV Au-Au collisions and (a) 83-93% centrality (\sim N-N collisions) and (c) 0-5% centrality. Histograms from 62 GeV collisions have the same general features with quantitative differences. Right: Two-dimensional model fits to histograms in the left panels without the BEC-electron component.

elliptic flow [15]. However, alternative mechanisms have been proposed [13, 34]. The narrow exponential represents Bose-Einstein correlations and electron pairs from photoconversions, and the narrow 1D peak on η_Δ is attributed to projectile nucleon dissociation. Reinterpretation of the NJ quadrupole based on comparison with jet-related systematics is a main subject of this study.

B. Two-dimensional fit model

In this study we emphasize correlation components (a), (b) and (c). The corresponding 2D model function is [7, 8, 23]

$$\frac{\Delta\rho}{\sqrt{\rho_{ref}}} = A_0 + A_{2D} \exp \left\{ -\frac{1}{2} \left[\left(\frac{\phi_\Delta}{\sigma_{\phi_\Delta}} \right)^2 + \left(\frac{\eta_\Delta}{\sigma_{\eta_\Delta}} \right)^2 \right] \right\} + A_D \{1 + \cos(\phi_\Delta - \pi)\}/2 + A_Q 2 \cos(2\phi_\Delta). \quad (2)$$

A 1D Gaussian on η_Δ (soft component, negligible in more-central Au-Au collisions) and 2D exponential (very narrow in more-central Au-Au collisions) are omitted from Eq. (2) for simplicity but were included in the analyses of Refs. [7, 23]. Equation (2) is a more-detailed version of Eq. (1).

Nonjet quadrupole measure A_Q as defined by Eq. (2) is statistically compatible with jet-related measures A_{2D} and A_D (all are per-particle measures), permitting quantitative comparisons between jet-related and non-jet quadrupole systematics. The quadrupole amplitude

is related to conventional measure $v_2\{2D\}$ by $A_Q\{2D\} = \rho_0(b) v_2^2\{2D\}$, where $\rho_0(b) = dn_{ch}/2\pi d\eta$ is the single-particle 2D angular density and symbol $\{2D\}$ denotes parameters inferred from 2D model fits to angular correlations as described in Refs. [7, 13, 14, 23].

IV. TWO-DIMENSIONAL MODEL FITS

Figure 1 (right panels) shows typical 2D model fits compared to corresponding data histograms in the left panels. For each data histogram fits are initiated from many different combinations of initial starting parameters (typically 100-1000) to insure achievement of global χ^2 minima. The fit residuals are typically consistent with bin-wise statistical uncertainties. The general evolution with centrality is monotonic increase of the SS 2D peak and AS dipole amplitudes (jet-related structures), substantial increase of the SS peak η_Δ width, rapid decrease to zero of the 1D Gaussian on η_Δ [7–9] and non-monotonic variation of the nonjet quadrupole [23].

A. Jet-related structures

Figure 2 shows fit results for jet-related structures from Ref. [7] where they are extensively discussed. The dashed curves in the upper panels indicate a Glauber linear superposition (GLS) trend expected for transparent A-A collisions. The jet-related amplitudes follow that trend from N-N collisions to a *sharp transition* at $\nu \approx 3$ corresponding to $\sigma/\sigma_0 \approx 50\%$. Above that point the amplitudes increase relative to the GLS trend in a manner consistent with a modification of parton fragmentation that conserves parton energy within resolved jets [17, 35].

Figure 2 (lower panels) show the η and ϕ widths of the SS 2D peak. Strong elongation on η of the SS peak in more-central Au-Au collisions was first reported in Ref. [8]. The physical mechanism for elongation is currently intensely debated [36, 37]. It is notable that the SS peak azimuth width actually *decreases* with increasing centrality. Mechanisms for jet modification and/or parton energy loss that rely on multiple scattering and/or gluon bremsstrahlung must confront that decrease.

B. Nonjet quadrupole

Figure 3 summarizes 2D fit results for $A_Q\{2D\}(b)$ (left panel) and corresponding values of $v_2\{2D\}(b)$ (right panel) for comparison with published v_2 measurements. The left panel shows fit results for 200 GeV (solid dots) and 62 GeV (open circles) data: strong increase to mid-central collisions followed by reduction to zero for central collisions. In the right panel the v_2 trend suggests substantial “elliptic flow” for the most-peripheral centrality bin approximating N-N collisions. The solid and dashed curves are defined in the next subsection. The dashed

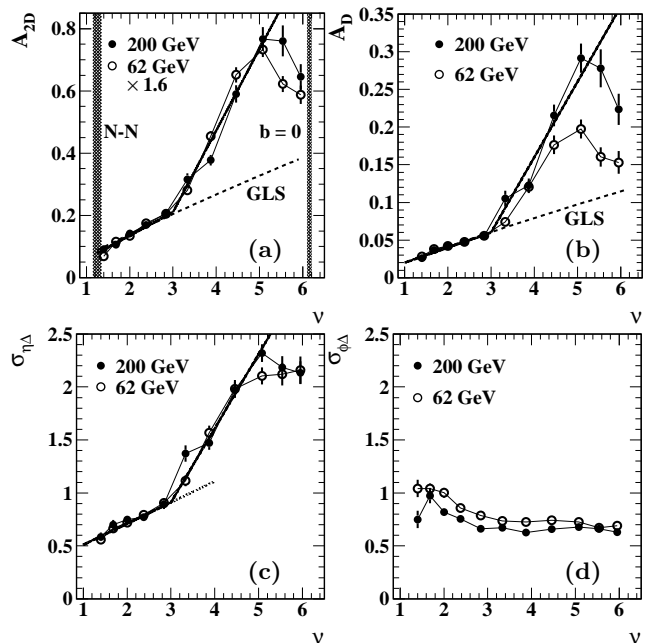


FIG. 2: Centrality dependence of fit parameters from Eq. (2) for (a) same-side (SS) 2D peak amplitude, (b) away-side (AS) 1D peak amplitude, (c) SS peak η width, (d) SS peak ϕ width.

curves correspond to NA49 $v_2\{EP\}$ measurements at 17 GeV (see Sec. IV D) that provide a reference for inferred energy-dependence systematics.

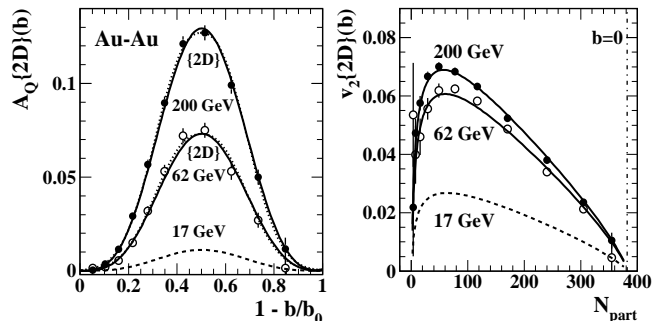


FIG. 3: Left: Nonjet quadrupole amplitude $A_Q\{2D\}(b)$ plotted on relative impact parameter $b/b_0 = \sqrt{\sigma/\sigma_0}$ with $b_0 \approx 14.7$ fm. Right: Corresponding values for $v_2\{2D\}(b)$. The solid and dashed curves are defined by Eq. (3)

The plotting format in the left panel reveals an interesting centrality trend common to all energies between 13.5 GeV and 200 GeV: $A_Q(b)$ data approximate a Gaussian trend on relative impact parameter b/b_0 ($b_0 \approx 14.7$ fm for Au-Au collisions). The dotted curves just visible behind the solid curves are modified Gaussians symmetric about the midpoint [56].

The plotting format in the right panel is the more conventional $v_2(b)$ vs $N_{part}(b)$. Both the correlation measure and centrality measure are questionable. Correlation measure v_2 is the square root of per-pair measure v_2^2

actually extracted from pair ratio $\Delta\rho/\rho_{ref}$. If the physics of central Au-Au collisions were not different from p - p collisions (Glauber linear superposition) v_2 must scale as $1/\sqrt{n_{ch}}$. Thus, a general decrease of v_2 with centrality conveys no new information. It is variations *relative* to the $1/\sqrt{n_{ch}}$ trend that may be interesting.

Centrality measure N_{part} biases the visual presentation to favor the more-central 50% of the Au-Au fractional cross section σ/σ_0 . $N_{part} = 50$ approximates the 50% point on σ/σ_0 . As shown below, interesting changes in jet systematics occur near $N_{part} = 50$ [7] that are effectively concealed by the N_{part} centrality measure. The lower half of the fractional cross section provides an essential reference and should be made visually accessible. Such access is necessary for proper interpretation of non-jet quadrupole data in relation to jet data. Alternative centrality measures include b/b_0 (left panel), fractional cross section σ/σ_0 and mean participant path length ν .

C. Combining energy and centrality trends

The data in Fig. 3 (left panel) reveal two interesting features: (a) Data for all energies above 13 GeV are described by the same centrality variation (solid and dashed curves), and (b) the quadrupole amplitude scales with energy approximately as $\log(\sqrt{s_{NN}})$. A similar energy scaling was observed for $\langle p_t \rangle$ fluctuations/correlations attributed to minijets [10]. An algebraic model describing quadrupole energy and centrality trends (solid and dashed curves) is now derived.

Figure 4 (left panel) shows the trend on collision energy of $A_Q(b)$ maximum values at $b/b_0 \approx 0.5$. Published v_2 measurements have been converted to A_Q values based on corresponding multiplicity densities and the relation $A_Q = \rho_0 v_2^2$. We observe two energy regimes: Below 13.5 GeV (Bevalac-AGS) the A_Q values are small and evolve with energy from negative to positive in response to the kinematic influence of spectator nucleons. The dashed line is defined by energy scaling factor $R'(\sqrt{s_{NN}}) \equiv \ln(\sqrt{s_{NN}}/3.2 \text{ GeV})$ with coefficient 0.008. Above 13.5 GeV (SPS-RHIC) the rate of increase becomes dramatically larger. The solid line is defined by scaling factor $R(\sqrt{s_{NN}}) \equiv \ln\{\sqrt{s_{NN}}/13.5 \text{ GeV}\}/\ln(200/13.5)$ with intercept $13.5 \pm 0.5 \text{ GeV}$ and coefficient 0.13 ± 0.01 .

Figure 4 (right panel) shows A_Q data plotted in the form $(1/\epsilon_{opt}^2)A_Q\{2D\}(b)$ vs $R(\sqrt{s_{NN}})N_{bin}(b)$, where N_{bin} is the number of binary N-N collisions and ϵ_{opt} is the eccentricity derived from an *optical* Glauber simulation [13, 38]. We observe empirically that for all Au-Au collisions above 13 GeV the $A_Q\{2D\}$ data are described accurately by the relation (solid line)

$$A_Q\{2D\}(b, \sqrt{s_{NN}}) = C_0 R(\sqrt{s_{NN}}) N_{bin}(b) \epsilon_{opt}^2(b). \quad (3)$$

Coefficient C_0 is defined by $1000C_0 = 4.5 \pm 0.2$. Equation (3) accurately describes the measured p_t -integrated nonjet azimuth quadrupole in Au-Au collisions for all centralities down to N-N collisions and all energies down

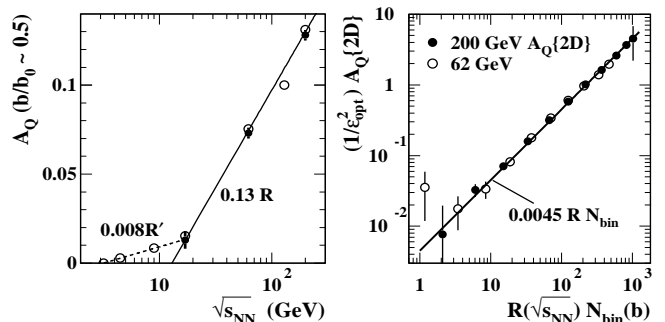


FIG. 4: Left: The energy dependence of azimuth quadrupole amplitude $A_Q = \rho_0 v_2^2$ evaluated at the maximum of that parameter on centrality. The trend $0.13R(\sqrt{s_{NN}})$ (solid line) defined above is included in Eq. (3). Right: Nonjet quadrupole data (points) for 62 and 200 GeV Au-Au compared to the trend defined by Eq. (3) (straight line).

to $\sqrt{s_{NN}} \sim 13 \text{ GeV}$. It defines the solid and dashed curves in Fig. 3.

D. Comparisons with other methods

NGNM v_2 measurements are conventionally interpreted to represent some combination of “elliptic flow” and “nonflow” [6] with several proposed sources for the latter such as resonances, Bose-Einstein correlations and jets [15]. Separating sinusoids attributed to “flow” from other correlation structure is a long-standing problem not resolved by non-graphical methods. Various strategies have been proposed to reduce “nonflow,” including cuts on η to exclude an interval on η_Δ containing the origin. The most common methods and their biases have been compared to 2D model fits on $(\eta_\Delta, \phi_\Delta)$ [13, 14, 22, 29, 39].

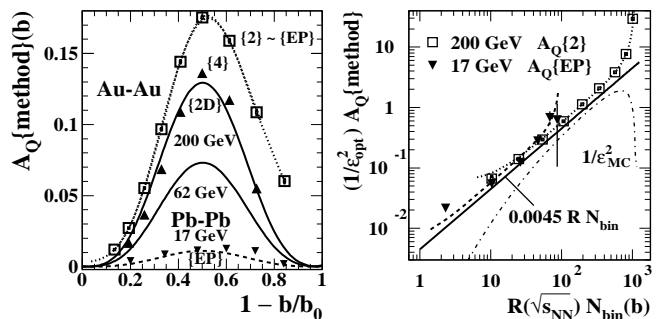


FIG. 5: Left: Quadrupole results from 2D model fits presented in Fig. 3 (solid and dashed curves) compared to published v_2 measurements obtained with other methods (points). The dotted curve includes a jet-related contribution obtained from the measured SS 2D peak systematics in Fig. 2. Right: 2D model-fit trend from Eq. (3) (solid line) compared to published v_2 measurements from other methods (points). The dotted and dashed curves include a calculated contribution from the measured SS 2D peak.

Figure 5 (left panel) shows multiparticle cumulant

measurements $A_Q\{2\}$ (open squares) and $A_Q\{4\}$ (solid upright triangles) from 200 GeV Au-Au collisions [15] and event-plane measurements $A_Q\{EP\}$ (solid inverted triangles) from 17 GeV Pb-Pb collisions [40] compared with Eq. (3) (solid and dashed curves). In Ref. [14] it was demonstrated that $v_2\{2\} \approx v_2\{EP\}$ to within 5% (consistent with experiment [15]). “Nonflow” contributions to those methods are discussed in App. A. Published uncertainties for the $A_Q\{2\}$ measurements multiplied by factor 10 to make them visible are shown as bars within the open squares. It is claimed that $v_2\{4\}$ eliminates “nonflow” arising from small clusters of particles (e.g., jets) [20, 21], and those measurements are indeed closer to the $A_Q\{2D\}$ trend (solid curve), but there are still very significant differences. The NA49 $v_2\{EP\}$ measurements (inverted triangles) [40] provide a reference for the energy-dependence systematics.

Figure 5 (right panel) shows the $A_Q\{2\}$ and $A_Q\{EP\}$ measurements compared with Eq. (3) (solid line). Deviations of the NGNM measurements from the linear trend are consistent with expected bias contributions from jet structure (SS 2D peak) [13] as described in App. A. The dotted curve passing through the 200 GeV measurements is a combination of Eq. (3) with jet-related contribution $A_Q\{SS\}$ derived from jet-related correlation properties presented in Sec. IV A. The same procedure generated the dotted curve in the left panel. The dashed curve approximating the 17 GeV measurements includes the same jet-related $A_Q\{SS\}$ contribution scaled down with energy according to $R(\sqrt{s_{NN}})$ from Eq. (3). The dash-dotted curve indicates what the $A_Q\{2D\}$ data trend (solid line) would be if ϵ_{opt} were replaced by Monte Carlo ϵ_{MC} . The Monte Carlo eccentricity trend appears to compensate partially for the jet contribution to $A_Q\{2\}$.

V. QUADRUPOLE VS JET TRENDS

A unique finding of Ref. [7] was the “sharp transition” separating Glauber linear superposition and apparent A-A transparency within the more-peripheral half of the total cross section and strong deviations from the GLS trend still consistent with a pQCD description within the more-central half. The NJ quadrupole data reported in Ref. [23] demonstrated remarkably simple energy and centrality trends for all Au-Au (or Pb-Pb) centralities and all energies above 13 GeV. We make direct comparisons between jet-related systematics and the nonjet quadrupole. We emphasize the relation of data trends to initial-state geometry parameters and possible QCD mechanisms.

A. Minimum-bias jet systematics

Figure 6 shows jet-related SS 2D peak A_{2D} (Gaussian) and AS 1D peak A_D (dipole) amplitudes vs centrality measured by fractional cross section. The hatched bands

show the position of the “sharp transition” (ST) near 50% ($\nu \approx 3$ or $N_{part} \approx 50$). The per-particle peak amplitudes A_X are rescaled by factor n_{ch}/N_{bin} because those hard-component amplitudes are expected to scale with N_{bin} (as described in Sec. II F). The covariance in the numerator of $\Delta\rho/\sqrt{\rho_{ref}}$ is then compared directly with the number of initial-state N-N binary collisions rather than the number of final-state hadrons. We observe that below the ST the “jet-related” amplitudes are systematically consistent with a constant value as expected for dijet production in a transparent system, thereby buttressing the jet interpretation. Above the ST the amplitudes increase substantially relative to the GLS trend.

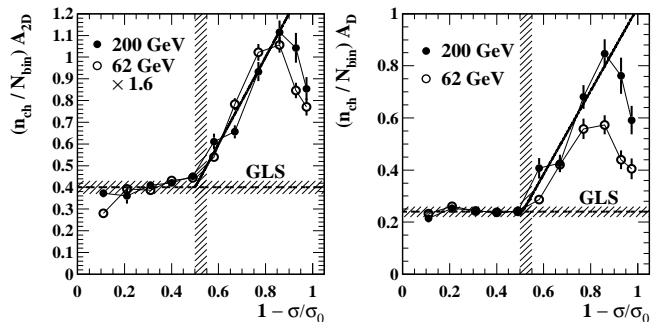


FIG. 6: Left: Same-side 2D peak amplitude vs fractional cross section. The amplitude has been rescaled to compare the covariance to the number of binary N-N collisions. Right: Away-side 1D peak amplitude rescaled in the same way. The constant trends are consistent with pQCD dijet production in transparent A-A collisions. The hatched bands mark a sharp transition in jet-related systematics.

In the left panel the SS peak amplitudes for 62 GeV rescaled by factor 1.6 [$\approx 1/R(62 \text{ GeV}) = 1.75$] are then equivalent to the 200 GeV amplitudes. In the right panel the unrescaled AS peak amplitudes for the two energies agree closely within the GLS interval. For in-vacuum dijets we expect the SS peak amplitude (sum of individual jets projected onto 1D y_z) to exhibit a $\log(\sqrt{s_{NN}})$ trend due to the increase of the kinematically-allowed longitudinal rapidity y_z interval, whereas the AS peak amplitude [representing the dijet density on 2D (y_{z1}, y_{z2})] should increase more slowly or not at all with energy [35, 41]. We observe such trends within the transparency interval. Thus, comparison of SS and AS centrality and energy trends strongly buttresses a dijet interpretation for those correlation structures, but also reveals a significant change in some jet-related correlation properties above the ST. The substantial increase of jet-related amplitudes (and SS η width) above the ST corresponds quantitatively to possible changes in parton fragmentation that still conserve the full parton energy within the resolved jet structure [43]. That description is supported by spectrum analysis [17, 33] and correlation analysis [35].

B. Nonjet quadrupole systematics

Figure 7 (left panel) shows quadrupole amplitude $A_Q\{2D\}$ with the 62 GeV data rescaled by factor $1/R(62\text{ GeV}) = \ln(200/13.5)/\ln(62/13.5) = 1.75$. The close overall agreement is consistent with Eq. (3). The point-to-point agreement demonstrates the accuracy of the analysis method, with deviations at the few-percent level for two distinct data volumes. The hatched band represents the sharp transition in jet properties. It is remarkable that in the more-peripheral centrality interval, where 3 GeV partons manifest as in-vacuum jets (hadron $\langle p_t \rangle \approx 1\text{ GeV}/c$) with no modification and we describe A-A collisions as *transparent*, the nonjet quadrupole conventionally interpreted to represent “elliptic flow” of a dense, strongly-interacting QGP increases to 60% of the maximum value as measured by $A_Q\{2D\}$ or the maximum value as measured by $v_2\{2D\}$ in Fig. 3 (right).

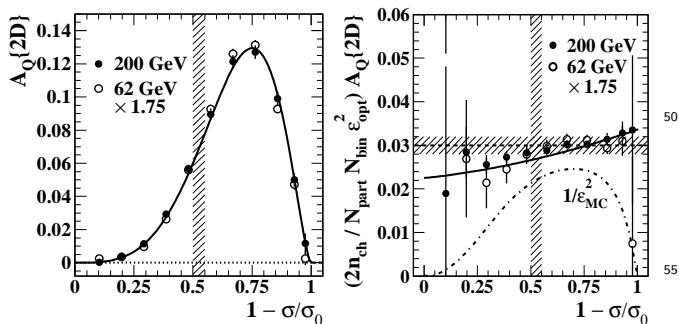


FIG. 7: Left: Azimuth quadrupole amplitudes vs fractional cross section. The 62 GeV data are scaled up according to factor $1/R(\sqrt{s_{NN}}) = 1.75$ and coincide at the percent level with the 200 GeV data. The curve is Eq. (3). The hatched band indicates that the nonjet quadrupole achieves 60% of its maximum amplitude within transparent A-A collisions. Right: A_Q data rescaled to participant nucleon pairs and further rescaled according to Eq. (3). Both the rescaled and unrescaled data are systematically consistent with Eq. (3). The dash-dotted curve shows the data trend resulting from rescaling with ϵ_{MC} instead of ϵ_{opt} .

Figure 7 (right panel) shows a variant of Fig. 4 (right panel) in which the A_Q data are first rescaled by factor $2n_{ch}/N_{part}$ to compare the quadrupole covariance in the numerator to initial-state participant pairs rather than final-state hadrons and then by factor $1/N_{bin}\epsilon_{opt}^2$ corresponding to Eq. (3). The data are systematically consistent with a constant value (dashed line). The solid curve represents the same rescaling applied to the Eq. (3) expression for A_Q and is also consistent with the data.

Figure 3 (right panel) shows $v_2\{2D\} = 0.022$ for the most peripheral 200 GeV centrality bin (approximately N-N collisions). In Fig. 7 that N-N value is consistent with a simple scaling trend describing all Au-Au centralities. It is also notable that $v_2\{2D\}$ in the N-N limit of Au-Au collisions is consistent with a pQCD color-dipole prediction $v_2 \approx 0.02$ for pions from p - p collisions [34].

Collision eccentricity can also be modeled by a *participant-nucleon* or *Monte Carlo* Glauber simulation [13]. The so-called Monte Carlo eccentricity ϵ_{MC} rises well above ϵ_{opt} for peripheral and central collisions because of point-like sampling of the nuclear volume [44]. In Fig. 7 (right) if ϵ_{MC} replaced ϵ_{opt} sharp downturns in the data would appear at the centrality extremes (dash-dotted curve) contradicting any possibility of a conjectured “hydro limit” for v_2 in central Au-Au collisions [45].

VI. DISCUSSION

We summarize and compare several aspects of jet-related correlations and jet and nonjet quadrupole data systematics and consider alternative interpretations of the nonjet quadrupole in light of inconsistencies in the conventional “elliptic flow” hydrodynamic interpretation.

A. 2D model fits compared to other v_2 methods

The azimuth quadrupole $A_Q\{2D\}$ or $v_2\{2D\}$ data used in this study are obtained from 2D model fits to angular correlations, but the majority of published v_2 measurements are obtained from various nongraphical numerical methods (e.g., $v_2\{2\}$, $v_2\{4\}$, $v_2\{EP\}$). It could be argued that the 2D fit model is somehow arbitrary, that it “depends on assumptions” (e.g., choice of model function for the SS 2D peak), and that the inferred quadrupole amplitudes are then uninterpretable and should be ignored [46]. But such arguments imply that NGNM aren’t based on model fits and don’t “depend on assumptions.”

Detailed study of NGNM reveals direct algebraic connections between such methods and 2D angular correlation histograms, and therefore 2D model fits to those histograms [13, 14, 30]. In fact, most NGNM are actually based on cosine model fits to 2D angular correlations projected onto 1D azimuth while subjected to various conditions on accepted particle pairs, including constraints on η difference acceptance and charge combination.

The NGNM fit model is effectively a single cosine which *cannot accurately describe* the 1D projection. The fit residuals are not examined to test the fit validity, and the procedure abandons critical information contained in the unprojected 2D angular correlations. The fitted cosine amplitude (assumed to represent “flow”) can then include contributions from multiple correlation components, some identified as “nonflow.” Assumptions supporting NGNM methods include identification of any cosine term as representing a flow [22, 29, 47, 48] and that “azimuthal anisotropy” (any nonuniform structure on azimuth) is dominated by, if not exclusively, flows [6].

In contrast, the same 2D fit model defined in Refs. [7, 23] is constrained to describe all 2D data from p - p collisions to central Au-Au collisions. The model is based only on observed prominent features of the data, not on physical assumptions. In p - p and more-peripheral Au-Au

collisions the SS 2D peak is fully resolved and the data require a SS 2D Gaussian model. The remaining structure (aside from the soft component and BEC) is fully described by two terms of a Fourier series according to inspection of the fit residuals. The two Fourier amplitudes have very different systematic variations on energy and centrality, suggesting minimal parameter covariance. In more-central Au-Au collisions the SS peak persists as a narrow structure on azimuth consistent with a Gaussian.

Systematic uncertainties in the azimuth quadrupole arising from 2D model choices are negligible in the GLS region where the SS 2D peak is fully resolved. In more-central Au-Au collisions it can be shown that the non-jet quadrupole amplitude is insensitive to the SS peak η structure as long as a SS Gaussian on azimuth is included in the model. Accurate separation of the three major correlation components is confirmed by the internal consistency of the parameter trends. Model comparisons are discussed further in App. A.

B. Jet correlation systematics

Figure 6 shows data for the SS 2D peak (left) and AS 1D peak (right) amplitudes scaled by factor (n_{ch}/N_{bin}) to determine the ratio of nominally jet-related covariances to number of initial-state N-N binary collisions rather than final-state hadrons. The data are plotted vs fractional cross section to emphasize an important point. Within the lower 50% of the total cross section the SS and AS data agree precisely with binary-collision scaling as expected for dijet production in transparent Au-Au collisions, supporting the dijet interpretation. The most-probable jets emerge from the lowest-energy partons that can appear as jets in the final state (approximately 3 GeV), as demonstrated in Refs. [7, 16–19]. Such low-energy partons (serving as “Brownian probes”) should be most susceptible to a dense, strongly-interacting medium. The data are consistent with no jet modification or medium formation in the more-peripheral half of the total cross section.

Just above the 50% point (“sharp transition”) the jet-related amplitudes increase substantially relative to the constant GLS trend, the deviation described as “anomalous centrality variation” in Ref. [7]. But the increase remains consistent with pQCD calculations incorporating modification of fragmentation functions in more-central Au-Au collisions that conserves the parton energy within resolved jets [17, 35]. The fragment yield increase at lower p_t (e.g., 0.5 GeV/c) is precisely anticorrelated with so-called “jet suppression” at larger p_t (e.g., 10 GeV/c) [33]. Jet modification in more-central collisions is not suppression of jet number but rather redistribution of fragment number along the jet axis from higher p_t to lower p_t [17]. We conclude that some aspects of parton fragmentation to minimum-bias jets inferred from spectrum analysis and 2D model fits to p_t -integral angular correlations remain consistent with a pQCD jet descrip-

tion from p - p to central Au-Au collisions.

C. Quadrupole correlation systematics

In Fig. 7 (left panel) we demonstrate precise consistency of 62 and 200 GeV $A_Q\{2D\}$ data scaled by a common $\log(\sqrt{s_{NN}})$ energy dependence shown in Fig. 4 (left panel) and similar to that observed for dijets [10]. Compared to the energy dependence below 13.5 GeV the rate of increase above 13.5 GeV is very large (slope changes by more than a factor 20). The actual increase in *collectivity* below 13.5 GeV is smaller than what the data there suggest due to the kinematic effect of spectator nucleons (“squeezeout”) resulting in negative values at lower energies. Whereas most particles participate in collective motion at lower energies, analysis of $v_2(p_t)$ data to infer “quadrupole p_t spectra” at 200 GeV [30] suggests that only a small fraction of final-state hadrons participates in the nonjet quadrupole at higher energies and must therefore be very strongly correlated to produce observed $A_Q\{2D\}(p_t, b)$ amplitudes at RHIC energies [12, 49].

In Ref. [23] it was demonstrated that $A_Q\{2D\}$ data vary approximately as $N_{bin}\epsilon_{opt}^2$. In the right panel A_Q is rescaled as $(n_{ch}/N_{part})(1/N_{bin}\epsilon_{opt}^2)$. The rescaled data are again consistent with a constant value (dashed line) within $\pm 10\%$ (hatched band), and the data for two energies are consistent within a few percent, although the absolute A_Q values vary over nearly three decades.

D. Jet-quadrupole comparisons

By comparing Fig. 6 and Fig. 7 (left panel) we observe that A_Q attains 60% of its maximum value within a centrality interval (more-peripheral 50% of σ/σ_0) that is effectively transparent to jet formation from low-energy (mainly 3 GeV) partons, an interval where multiple (re)scattering of partons or hadrons apparently plays no significant role. Within the transparency interval we observe that whereas the jet-related covariance scales as N_{bin} (as expected for pQCD dijet production) the nonjet quadrupole covariance scales as $N_{part} \times N_{bin} \times \epsilon_{opt}^2$, faster than dijet production in more-peripheral collisions.

Figure 7 (right panel) shows that the nonjet quadrupole continues to follow the same simple algebraic trend within $\pm 10\%$ through and above the sharp transition, where the minimum-bias jet trends change dramatically and where substantial modification of jet formation appears [7]. The quadrupole seems to be completely insensitive to whatever mechanism modifies jet structure.

E. Implications for hydro interpretations

What are the implications from these observations for hydro interpretations of the azimuth quadrupole? v_2 measurements have been conventionally interpreted in

a hydro context in terms of ratio v_2/ϵ plotted vs low-density limit (LDL) parameter $dn_{ch}/d\eta S$ [45, 50] (S is the A-A overlap area). For more-peripheral collisions it is expected that $v_2/\epsilon \propto dn_{ch}/d\eta S$ (assumed correlated with the mean number of particle rescatterings during equilibration). If thermal equilibrium is achieved the *ideal-hydro limit* $v_2/\epsilon \rightarrow$ constant (saturation) is expected. Previous v_2 measurements were believed to confirm that central Au-Au collisions at 200 GeV achieve the ideal-hydro limit (thermalization over some substantial space-time volume) [50, 51].

Conventional v_2 analysis is based on assumptions that hydro expansion with particle rescattering is the dominant dynamical process in heavy ion collisions [3, 51], that the collision can be described in part as a thermodynamic state [52], and v_2 is sensitive to an equation of state [4, 5]. v_2 is defined accordingly [3, 6], and nonflow contributions to v_2 are estimated with physical-model-dependent procedures [15, 20, 21]. The present analysis presents accurate nonjet quadrupole amplitudes from physical-model-independent 2D fits to angular correlations that reveal simple trends on centrality and collision energy, including factorization of the dependence on collision parameters b (impact parameter) and $\sqrt{s_{NN}}$.

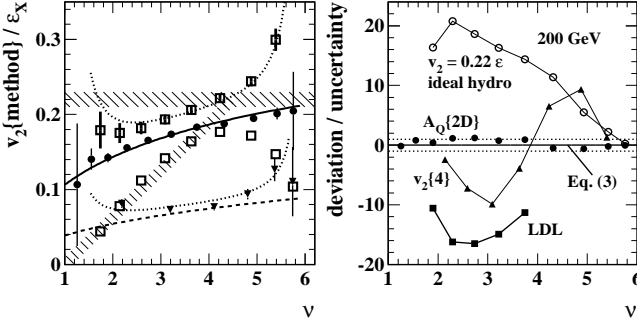


FIG. 8: Left: Ratios v_2/ϵ for various combinations of $v_2\{\text{method}\}$ and ϵ_X with $X = \text{opt}$ or MC . The solid and dashed curves are Eq. (3) for 200 and 17 GeV. $v_2\{2\}$ measurements for 200 GeV are open squares [15] [published uncertainties (bars) are multiplied by factor 20 for visibility]. $v_2\{EP\}$ measurements for 17 GeV are solid triangles [40]. The dotted lines are Eq. (3) plus a calculated contribution from the jet-related SS 2D peak. Right: Deviations [data - Eq. (3)] relative to systematic uncertainties for 200 GeV 2D model-fit measurements (solid dots), and for $v_2\{4\}$ (solid triangles), ideal-hydro $v_2/\epsilon = 0.22$ (open circles) and LDL $v_2/\epsilon = 0.01$ ($dn_{ch}/d\eta S$) (solid squares). $v_2\{\text{method}\}$ values are converted to $A_Q = \rho_0 v_2^2$.

Figure 8 (left panel) shows ratio v_2/ϵ for several v_2 methods ($v_2\{2\}$ open squares, $v_2\{EP\}$ solid triangles and $v_2\{2D\}$ solid dots) and two ϵ calculations (ϵ_{opt} optical and ϵ_{MC} Monte Carlo). The vertical scale choice excludes a $v_2\{2\}/\epsilon_{\text{opt}}$ point at 0.55 for central Au-Au to retain sufficient resolution for the other data. The data points and line types are consistent with Fig. 5 (left panel). The solid curve is Eq. (3) including ϵ_{opt} . The upper dotted curve is the solid curve plus the contribu-

tion from the SS 2D (jet) peak calculated in App. A. The dashed curve represents Eq. (3) for 17 GeV with ϵ_{opt} , and the lower dotted curve is that plus the jet contribution from 200 GeV scaled down by factor $R(17 \text{ GeV})$. The bars in the upper open squares represent the published $v_2\{2\}$ systematic uncertainties multiplied by factor 20. The lower open squares are the same $v_2\{2\}$ measurements but combined with ϵ_{MC} . The upper hatched band represents an ideal-hydro saturation limit predicted for 200 GeV. The lower hatched band sketches an LDL trend on v . Incorporation of ϵ_{MC} in the v_2/ϵ ratio partially compensates for the jet contribution to $v_2\{2\}$ and seems to meet LDL expectations for more-peripheral collisions. But the accompanying downturn for more-central collisions contradicts hydro expectations for saturation.

Figure 8 (right panel) compares data and theoretical expectations in the form of deviations from Eq. (3) divided by data systematic uncertainties (“error” bars). The $v_2\{2D\}$ data (solid dots) are systematically consistent with Eq. (3) as expected. The $v_2\{4\}$ measurement deviations relative to their published uncertainties [21] reveal systematic deviations of either sign up to ten uncertainty bars from Eq. (3). The ideal-hydro $v_2/\epsilon = 0.22$ and LDL-scaling $v_2/\epsilon \approx 0.01$ ($dn_{ch}/d\eta S$) also exhibit large deviations (relative to uncertainties in $v_2\{2D\}$ data).

The more-peripheral NJ quadrupole data do not appear to follow an LDL trend or require subsequent Au-Au collision evolution by particle (parton or hadron) rescattering, and no transition to an ideal-hydro limiting case is observed. The $A_Q\{2D\}$ data do not compel a model description based on bulk-medium hydrodynamics or an equation of state, in fact contradict such descriptions.

Thus, the measured $A_Q\{2D\}$ data trends, especially the entire energy-dependence trend at and above Bevalac energies, the complete insensitivity of the nonjet quadrupole to jet modifications in more-central Au-Au collisions and detailed understanding of jet-related contributions to $v_2\{\text{method}\}$ measurements (i.e., required corrections for jet-related “nonflow” bias) strongly suggest that the conventional hydro interpretation of the nonjet quadrupole as “elliptic flow” is contradicted by most v_2 measurements.

F. Hydrodynamic flows vs alternative mechanisms

Other analysis results argue against hydrodynamic flows in high energy nuclear collisions [12]. Published $v_2(p_t)$ measurements for identified hadrons reveal a *quadrupole p_t spectrum* common to three hadron species and consistent with a boosted source (a form of “radial flow”) but with a cold spectrum shape very different from that for the majority of final-state hadrons [49]. The inferred boost distribution is also inconsistent with Hubble expansion of a flowing bulk medium [30]. The combined spectrum characteristics suggest that the fraction of hadrons “carrying” the nonjet quadrupole is sub-

stantially less than 10%, ruling out an expanding bulk medium as the common source for most hadrons [49]. The systematics of $v_2\{2D\}(p_t, b)$ data reveal that the source boost does not depend on Au-Au centrality as one might expect for a hydro scenario [30].

Differential study of single-particle p_t spectra for identified hadrons reveals that spectrum structure conventionally interpreted with a “blast-wave” model in terms of radial flow [53] is actually consistent with parton fragmentation to jets for all Au-Au centralities [12, 17, 33]. The nonjet quadrupole has a substantial amplitude within the “transparency” centrality interval of Au-Au collisions, with nonzero values down to N-N collisions [7, 23]. The measured N-N quadrupole systematics extrapolated to LHC energies explain the same-side “ridge” in 7 TeV p - p collisions as a quadrupole manifestation [41, 42]. Thus, the nonjet quadrupole amplitude becomes large in collision systems where particle densities are still small, again contradicting a hydro scenario. If the nonjet quadrupole does not represent “elliptic flow” what is the alternative mechanism? Growing evidence suggest that the NJ quadrupole is a QCD phenomenon arising from low- x glue-gluon interactions leading to long-wavelength (multipole) radiation [13]. For example, a QCD calculation of interfering radiation from decays of two BFKL ladders predicts a long-range quadrupole structure in p-p and A-A collisions [54].

Although the centrality trends for jet-related SS peak properties and nonjet quadrupole are very different the two amplitudes, when measured with statistically equivalent quantities A_Q and A_{2D} , share the same $\log(\sqrt{s_{NN}})$ energy dependence characteristic of QCD scattering processes. Equation (3) reveals that the final-state nonjet quadrupole amplitude for (some fraction of) produced hadrons is simply determined by initial-state parameters $(\sqrt{s_{NN}}, b)$ over a large kinematic domain including N-N (p-p) collisions. There is no evidence for quadrupole sensitivity to intermediate processes (multiple rescattering, formation of a thermodynamic state, whatever mechanism modifies jet-related correlations above the ST) within A-A collisions. And a prediction $v_2 \approx 0.02$ for pions from 200 GeV p - p collisions based on a QCD color-dipole model [34] is consistent with the observed N-N limit $v_2\{2D\} \approx 0.02$ in Fig. 3 [7, 23].

VII. SUMMARY

In summary, 2D angular correlation data for Au-Au collisions at 62 and 200 GeV are employed to re-examine interpretations of the azimuth quadrupole as “elliptic flow” conventionally represented by symbol v_2 , a hydrodynamic response to the eccentricity of the initial-state A-A overlap region. Unlike most conventional v_2 methods, two-dimensional (2D) model fits to angular correlation data distinguish accurately between jet-related features and a *nonjet* quadrupole represented by symbol A_Q . The nonjet (NJ) quadrupole exhibits simple sys-

tematic trends on collision centrality and energy. The trend $A_Q \propto R(\sqrt{s_{NN}}) N_{bin}(b) \epsilon_{opt}^2(b)$ with $R(\sqrt{s_{NN}}) \propto \log(\sqrt{s_{NN}}/13.5 \text{ GeV})$ accurately describes NJ quadrupole data over a broad range of energies and all Au-Au centralities. All p_t -integrated NJ quadrupole data from 17 to 200 GeV are fully described by two A-A initial-state parameters.

In contrast, jet-related features exhibit Glauber linear superposition (GLS) trends (transparency) over the more-peripheral 50% of the Au-Au total cross section, consistent with unmodified dijet production proportional to N-N binary collisions. In more-central collisions jet-related amplitudes increase relative to the GLS trend but in a manner still consistent with pQCD when a simple alteration of fragmentation leading to jets is introduced. Within the transparency interval minimum-bias (mainly 3 GeV) jet characteristics indicate negligible parton or hadron rescattering that might contribute to hydrodynamic phenomena in a dense medium. Within the same centrality interval the nonjet quadrupole amplitude A_Q increases to 60% of its maximum value.

Comparison of conventional v_2 measurements with jet-related and nonjet-quadrupole systematics reveals substantial bias in much of the v_2 measurements due to jet-related contributions, the amount depending on the v_2 “method” invoked. Comparison of the energy and centrality trends inferred for the p_t -integral nonjet quadrupole with hydro expectations for “elliptic flow” reveals major disagreements. The ratio v_2/ϵ does not follow the number of in-medium rescatterings during equilibration (LDL scaling) for more-peripheral A-A collisions and does not transition to a near-constant ideal-hydro trend for more-central collisions and larger collision energies (ideal hydro limit). Quadrupole p_t spectra inferred from identified-hadron $v_2(p_t)$ data are very different from the spectra for most hadrons. A quadrupole-source boost distribution inferred from such measurements is inconsistent with Hubble expansion of a flowing bulk medium.

We conclude that: (i) NJ quadrupole and jet-related structures arise from two different mechanisms and can be accurately distinguished by 2D model fits. (ii) The NJ quadrupole appearing in more-peripheral (“transparent”) Au-Au collisions cannot arise from a hydro mechanism relying on many rescatterings. (iii) The same NJ quadrupole is insensitive to any mechanism or environment (dense medium) that might modify jet structure in more-central collisions as observed. (iv) Both jets and NJ quadrupole exhibit a similar $\log(\sqrt{s_{NN}})$ energy dependence, with threshold near 13 GeV, suggesting a common QCD framework for both phenomena. (v) The NJ quadrupole is not a hydrodynamic flow manifestation.

This work was supported in part by the Office of Science of the U.S. DOE under grants DE-FG03-97ER41020 (UW) and DE-FG02-94ER40845 (UTA).

Appendix A: Flows and nonflows

“Elliptic flow” (v_2) measurements rely on an assortment of analysis methods that encounter the common problem of distinguishing “flow” from “nonflow.” The present study demonstrates that jet structure can be distinguished accurately from a nonjet remainder that might represent “flow” if flow were relevant to high-energy nuclear collisions [7, 12, 13, 23, 30]. The distinction is achieved by 2D model fits to angular correlations. Such model fits are dismissed by some because they “depend on assumptions.” But (a) any mathematical analysis depends on assumptions—the question is the validity of what is assumed—and (b) NGNM measurements *also rely on model fits*.

The NGNM v_2 fit model is a cosine (or cosine plus constant) applied to a 1D projection onto azimuth of *all* 2D angular correlations. Different v_2 methods are distinguished by the conditions imposed on accepted pairs (charge combination, hadron species, η acceptance) in attempts to reduce “nonflow” bias to v_m based on *physical* assumptions. The fit residuals are not presented (but see comments on ZYAM subtraction below). Based on results from Ref. [7] the residuals for a 1D single-cosine model must be large. Some fraction of the jet structure *must* be included in NGNM v_2 measurements as a “nonflow” bias. The amount of jet-related bias depends on the “method.” The bias can be predicted accurately from 2D model fits if $v_2\{\text{method}\}$ is sufficiently well defined [23, 30].

1. System A vs System B

We can identify two descriptive systems. System A is based on the observation that within all 2D angular correlation data three prominent features or components labeled (a), (b) and (c) consist of a SS 2D peak, an AS dipole and an azimuth quadrupole not associated with (a). Those features persist for all A-A collision systems. We measure their characteristics with 2D model fits. No physical assumptions motivate that description.

pQCD provides the standard description of high energy nuclear collisions, a falsifiable theory that makes real predictions about what should be observed. Included in those predictions is the appearance of (a) and (b) in 2D angular correlations and their systematic properties. The correspondence between predictions and data *requires* interpretation of (a) and (b) as pQCD jet-related. The jet interpretation arises from and relies on an established physical theory. What remains is (c), the nonjet quadrupole distinct from (a) and (b) in all cases. Its interpretation is questioned. No falsifiable theory currently predicts all measured properties of the NJ quadrupole. Thus, System A can be represented by $\text{Data} = \text{pQCD}\{\text{jets}\} + \text{“nonjets”}$ and is the basis for Ref. [7] reporting minijet systematics.

System B is based on the primary assumption that

“flows” (collective motion shared by many particles) must play a major role in high energy nuclear collisions. But “flows” are not required by QCD to exist at higher energies. The nucleons participating in collective motion observed at the Bevalac are no longer relevant. High-energy collisions are dominated by the low-x gluons in the projectiles – either liberated in place to form “soft” hadrons or undergoing “hard” scattering to form dijets.

In System B “Flows” are associated with one or more cylindrical multipoles. Non-graphical numerical methods (NGNM) *based on physical assumptions* are developed to extract multipole amplitudes v_m interpreted to represent “flows.” The methods rely on a common assumption that “flows” can be modeled by cosines. NGNM methods (the fit models) do not recognize the existence of a SS (jet) peak in correlation data or the contributions that the SS peak must make to NGNM multipole amplitudes v_m . But the SS peak is the dominant source of “nonflow” in published v_m measurements. The network of v_m methods and assumptions is complex and changeable. System B is represented by $\text{Data} = \text{“flow”} + \text{“nonflow”} + \text{“other”}$ (“other” represents structure independent of the v_m “flow” multipole of interest) and is the basis for analysis in Ref. [46] and other dihadron correlation studies based on *ZYAM subtraction* [39].

2. Mapping from System A to System B

If a “flow” analysis method is sufficiently well-defined we can establish a quantitative relation between systems A and B and demonstrate that the cross terms are large for the usual “flow” methods. “Jets” from A is split between “flow,” “nonflow” and “other” in B. “Nonjets” is also split, and some of “nonjets” may appear in “nonflow.” There is no justification for assuming that “nonflow” + “other” includes all of “jets,” but that common assumption is the basis for ZYAM subtraction [39, 46].

All angular correlation data include a SS 2D peak [feature (a), part of “jets”]. The SS peak is always narrow on ϕ but is elongated on η in more-central Au-Au collisions [7]. The SS 2D peak projected onto 1D azimuth is actually a periodic peak array with a Fourier series equivalent. The Fourier amplitudes for given peak width are represented by factor $F_m(\sigma_{\phi_\Delta})$ for the m^{th} Fourier term (cylindrical multipole) [39]. Projection of the 2D peak onto 1D azimuth depends on its η width relative to the η acceptance $\Delta\eta$ and is represented by factor $G(\sigma_{\eta_\Delta}, \Delta\eta)$ [35]. The jet-related quadrupole amplitude derived from SS 2D peak properties is then defined by [22]

$$2A_Q\{SS\}(b) = F_m(\sigma_{\phi_\Delta})G(\sigma_{\eta_\Delta}, \Delta\eta)A_{2D}(b). \quad (\text{A1})$$

With that expression we can relate nonjet $A_Q\{2D\}$ and jet-related $A_Q\{SS\}$ quadrupole amplitudes in System A to “flow” and “nonflow” in System B. The expression for more-complex η -exclusion cuts is derived in Ref. [22].

Figure 9 (left panel) shows a parametrization of the centrality dependence of SS 2D peak amplitude $A_{2D}(b)$

and three quadrupole amplitudes related by [13]

$$A_Q\{2\} = A_Q\{2D\} + A_Q\{SS\}. \quad (\text{A2})$$

$A_Q\{2D\}$ (solid curve) is defined by Eq. (3) [23] and $A_Q\{SS\}$ (dashed curve) by Eq. (A1) using SS peak parameters (amplitude and widths) from Ref. [7]. $A_Q\{2\}$ (dotted curve) is then a *prediction* for measured $v_2\{2\} \approx v_2\{EP\}$ measurements that are derived from cosine fits to 1D projection onto azimuth of all 2D angular correlation structure (“flow”) [14, 15]. The dotted curve in the left panel appears (transformed) in the right panel and Fig. 5.

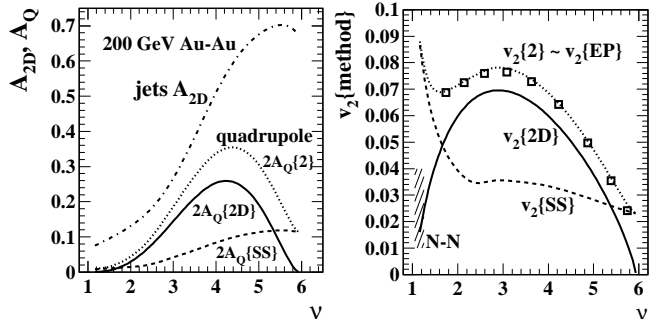


FIG. 9: Left: SS 2D (jet) peak amplitude A_{2D} (parametrization of data from Ref. [7]), SS 2D peak quadrupole component $A_Q\{SS\}$ (“nonflow,” inferred from Ref. [7] data) and nonjet quadrupole amplitude $A_Q\{2D\}$ from Eq. (3), with $A_Q\{2\} = A_Q\{2D\} + A_Q\{SS\}$ [13]. Right: Quadrupole amplitudes $A_Q\{X\}$ converted to conventional measures $v_2\{X\}$. The open squares are $v_2\{2\}$ measurements from Ref. [15]. The curves correspond to those in the left panel.

Figure 9 (right panel) shows $v_2\{X\}$ trends obtained from the corresponding $A_Q\{X\}$ curves in the left panel by $A_Q = \rho_0 v_2^2$. Also included are $v_2\{2\}$ measurements (open squares) from Ref. [15]. An equivalent comparison for 17 GeV measurements appears in Fig. 5. The precise agreement between measurements (points) and prediction (dotted curve) is evident. From the nonjet quadrupole trend and jet-related correlation structure in System A we accurately predict $v_2\{EP\} \approx v_2\{2\}$ published “flow” measurements in System B. The prediction does not include small contributions to $v_2\{2\}$ from BEC and electron pairs that are excluded from the SS peak $A_{2D}(b)$ data by the 2D model-fit procedure [7]. For statistically well-defined v_2 methods (e.g., $v_2\{2\} \approx v_2\{EP\}$) the “nonflow” (jet) bias contribution to inferred “flow” v_2 can be estimated accurately.

Attempts have been made to parameterize “nonflow” contributions to v_2 with quantity $g_2 = N_{part}[v_2^2\{2\} - v_2^2\{4\}]$ [15]. If we approximate $v_2\{4\}$ by $v_2\{2D\}$ we obtain $g_2 = (N_{part}/\rho_0)A_Q\{SS\} \approx \{5/[1 + 0.1(\nu - 1)]\}A_Q\{SS\}$. The factor in curly brackets is derived from a two-component model of particle production [32]. That expression agrees quantitatively with 200 GeV g_2 data in Fig. 31 of Ref. [15] except for more-peripheral collisions where $A_Q\{SS\}$ derived from 2D model fits does not include a relatively large contribution to $v_2\{2\}$ from BEC

and electron pairs. The comparison confirms the large “nonflow” contribution to $v_2\{2\}$ from the SS jet peak.

3. Consequences of System B

System B is the basis for dihadron correlation analysis on 1D azimuth including “ZYAM subtraction” of a combinatoric background. A “flow” background is estimated based on NGNM v_2 measurements and subtracted from Data (“raw” correlations). It is assumed that for some combination of v_2 methods the difference Data – “flow” = “nonflow” + “other” includes all of “jets.” The subtraction does reveal the large residuals of the System B model fit. After application of “trigger-associated” p_t cuts it is assumed that the surviving “nonflow” + “other” still retains all of “jets.” Since “flow” actually includes some fraction of “jets” (“nonflow”) the surviving “jets” structure in the ZYAM-subtracted and p_t -cut “nonflow” correlations is attenuated and distorted, leading to incorrect inferences about jet systematics [39]. The “nonflow” + “other” component in System B may include some fraction of “jets” from System A, but the fraction depends on arbitrary definitions of “flow” and “nonflow.”

Reference [46] presents a direct comparison between System A and System B. The ZYAM subtraction (System B) shown in Figs. 3 and 7 seems to indicate that with increasing angle relative to the EP from in-plane to out-of-plane the jet structure is increasingly attenuated and distorted, implying that “jet quenching” is directly correlated with the apparent parton path length in a “dense medium.” What survives ZYAM subtraction is then further separated into “jet-like” and “ridge-like” structure, again based on arbitrary assumptions. The paper concludes “...high p_t triggered jets are biased toward surface emission, and the jet fragmentation is hardly modified by the medium” (i.e., jets in central Au-Au collisions are the same in structure and abundance as in p - p collisions).

But Fig. 4 of that paper presents results from 1D model fits (System A), including a SS peak model element, that reveal undistorted jet structure. In contrast to severe jet attenuation and distortion with increasing angle inferred from System B the System A model fits reveal a possible increase of jet correlation amplitude and no distortions, consistent with the minijet analysis in Ref. [7] in which minijets are modified in more-central collisions, but in a manner consistent with pQCD expectations [17, 33, 35]. The System A results in Fig. 4 of Ref. [46] are dismissed there because v_2 systematics inferred from 1D model fits contradict “flow” v_2 inferred from NGNM analysis.

Any application of v_2 measurements to subsequent analysis requires a choice between (a) a comprehensive 2D fit model motivated by actual data structures combined with a few physical-model-independent assumptions and (b) an incomplete cosine model (NGNM) combined with many physical-model-dependent a priori assumptions. Choosing (a) may lead to interesting new physics derived within an intact QCD context represent-

ing a falsifiable theory. Choosing (b) (e.g., ZYAM subtraction) can lead to results that are distorted and mis-

leading.

-
- [1] J. Adams *et al.* (STAR Collaboration), Nucl. Phys. A **757**, 102 (2005).
- [2] P. Romatschke and U. Romatschke, Phys. Rev. Lett. **99**, 172301 (2007).
- [3] J. Y. Ollitrault, Phys. Rev. D **46**, 229 (1992).
- [4] D. Teaney, J. Lauret and E. V. Shuryak, Phys. Rev. Lett. **86**, 4783 (2001).
- [5] P. F. Kolb, U. W. Heinz, P. Huovinen, K. J. Eskola and K. Tuominen, Nucl. Phys. A **696**, 197 (2001).
- [6] A. M. Poskanzer and S. A. Voloshin, Phys. Rev. C **58**, 1671 (1998).
- [7] G. Agakishiev, *et al.* (STAR Collaboration), Phys. Rev. C **86**, 064902 (2012).
- [8] J. Adams *et al.* (STAR Collaboration), Phys. Rev. C **73**, 064907 (2006).
- [9] J. Adams *et al.* (STAR Collaboration), J. Phys. G **32**, L37 (2006).
- [10] J. Adams *et al.* (STAR Collaboration), J. Phys. G **34**, 451 (2007).
- [11] T. A. Trainor and D. T. Kettler, Phys. Rev. D **74**, 034012 (2006).
- [12] T. A. Trainor, J. Phys. G **37**, 085004 (2010).
- [13] T. A. Trainor, Mod. Phys. Lett. A **23**, 569 (2008).
- [14] T. A. Trainor and D. T. Kettler, Int. J. Mod. Phys. E **17**, 1219 (2008).
- [15] J. Adams *et al.* (STAR Collaboration), Phys. Rev. C **72**, 014904 (2005).
- [16] J. Adams *et al.* (STAR Collaboration), Phys. Rev. D **74**, 032006 (2006).
- [17] T. A. Trainor, Phys. Rev. C **80**, 044901 (2009).
- [18] R. J. Porter and T. A. Trainor (STAR Collaboration), J. Phys. Conf. Ser. **27**, 98 (2005).
- [19] R. J. Porter and T. A. Trainor (STAR Collaboration), PoS **CFRNC2006**, 004 (2006).
- [20] N. Borghini, P. M. Dinh and J. Y. Ollitrault, Phys. Rev. C **64**, 054901 (2001).
- [21] C. Adler *et al.* (STAR Collaboration), Phys. Rev. C **66**, 034904 (2002).
- [22] T. A. Trainor, arXiv:1109.2540.
- [23] D. T. Kettler (STAR collaboration), Eur. Phys. J. C **62**, 175 (2009).
- [24] J. Adams *et al.* (STAR Collaboration), Phys. Lett. B **634**, 347 (2006).
- [25] T. A. Trainor, R. J. Porter and D. J. Prindle, J. Phys. G **31**, 809 (2005).
- [26] K. H. Ackermann *et al.*, Nucl. Instrum. Meth. A **499**, 624 (2003).
- [27] J. L. Rodgers and W. A. Nicewander, "Thirteen ways to look at the correlation coefficient." The American Statistician **42**, 59 (1988).
- [28] B. S. Everitt and A. Skrondal, "The Cambridge Dictionary of Statistics," 4th Ed., (Cambridge University Press, Cambridge, 2010), p. 107.
- [29] T. A. Trainor, D. J. Prindle and R. L. Ray, Phys. Rev. C **86**, 064905 (2012).
- [30] D. Kettler (STAR Collaboration), J. Phys. Conf. Ser. **270**, 012058 (2011).
- [31] T. A. Trainor and D. J. Prindle, arXiv: hep-ph/0411217.
- [32] D. Kharzeev and M. Nardi, Phys. Lett. B **507**, 121 (2001).
- [33] T. A. Trainor, Int. J. Mod. Phys. E **17**, 1499 (2008).
- [34] B. Z. Kopeliovich, A. H. Rezaeian and I. Schmidt, Phys. Rev. D **78**, 114009 (2008).
- [35] T. A. Trainor and D. T. Kettler, Phys. Rev. C **83**, 034903 (2011).
- [36] T. A. Trainor, J. Phys. G **39**, 095102 (2012).
- [37] T. A. Trainor and R. L. Ray, Phys. Rev. C **84**, 034906 (2011).
- [38] The optical Glauber eccentricity is expressed on N_{bin} as $\epsilon_{opt} = 0.185[\log_{10}(3 N_{bin}/2)]^{0.96}[\log_{10}(1136/N_{bin})]^{0.78}$.
- [39] T. A. Trainor, Phys. Rev. C **81**, 014905 (2010).
- [40] A. M. Poskanzer *et al.* (NA49 Collaboration), Nucl. Phys. A **661**, 341 (1999).
- [41] T. A. Trainor and D. T. Kettler, Phys. Rev. C **84**, 024910 (2011).
- [42] R. L. Ray, Phys. Rev. D **84**, 034020 (2011).
- [43] N. Borghini and U. A. Wiedemann, hep-ph/0506218.
- [44] B. Alver *et al.* (PHOBOS Collaboration), Phys. Rev. Lett. **98**, 242302 (2007).
- [45] S. A. Voloshin and A. M. Poskanzer, Phys. Lett. B **474**, 27 (2000).
- [46] H. Agakishiev *et al.* (STAR Collaboration), arXiv:1010.0690.
- [47] B. Alver and G. Roland, Phys. Rev. C **81**, 054905 (2010).
- [48] M. Luzum, Phys. Lett. B **696**, 499-504 (2011).
- [49] T. A. Trainor, Phys. Rev. C **78**, 064908 (2008).
- [50] S. A. Voloshin (STAR Collaboration), AIP Conf. Proc. **870**, 691 (2006).
- [51] U. W. Heinz, "Early collective expansion: Relativistic hydrodynamics and the transport properties of QCD matter," in "Relativistic Heavy Ion Physics," Landolt-Boernstein New Series, I/23, edited by R. Stock (Springer Verlag, New York,2010) Chap. 5.
- [52] P. Huovinen and P. V. Ruuskanen, Ann. Rev. Nucl. Part. Sci. **56**, 163 (2006).
- [53] F. Retiere and M. A. Lisa, Phys. Rev. C **70**, 044907 (2004).
- [54] E. Levin and A. H. Rezaeian, Phys. Rev. D **84**, 034031 (2011).
- [55] The mean jet fragment multiplicity increases from ≈ 2.5 in p - p to ≈ 8 in central Au-Au collisions [16, 17, 33].
- [56] The functional form is $\exp\{-|(x - 0.5)/0.178|^{2.4}/2\}$.